Journal of
Nanoelectronics and Optoelectronics
Vol. 19, pp. 256–263, 2024
www.aspbs.com/jno

ARTICLE

Enhancing Hydrogen Sulfide Gas Detection: Tailoring ZnO Films Through a Novel Sol–Gel Approach with Ultra-Sonication

Sushil Charpe[1,*], Pranali Raut[2], Vijay Rahangdale[3], Praful Shirbhate[4], Rohit Agrawal[5], Mohamed H. Mahmoud[6], Nasser M. Abd El-Salam[7], and H. Fouad[6]

In this study, nano-sized Zinc Oxide (ZnO) particles were synthesized using a novel sol–gel process with $Zn(NO_3)_2$ solutions, specifically tailored for the development of a highly efficient Hydrogen Sulphide (H_2S) gas sensing element. The impact of ultra-sonication on the properties crucial for H_2S detection was systematically investigated. The resulting ZnO materials exhibited a well-defined crystalline structure along (100), (002), (101), and (102) planes, confirming the formation of the hexagonal wurtzite phase of ZnO. Significantly, an increase in sonication treatment time led to a reduction in particle size. The gas sensing properties for H_2S were meticulously analyzed in relation to the varying sizes of ZnO films. Remarkably, the ZnO film fabricated with a 30-minute ultra-sonication treatment demonstrated the highest response to H_2S gas at 423 K. The ZnO-thick films exhibited notable sensitivity, coupled with rapid reactivity and recovery times upon exposure to H_2S gas. Importantly, our findings establish a direct correlation between the sensitivity of the ZnO sensor and the particle size.

Keywords: ZnO Films, Sol–Gel Technique, Hydrogen Sulphide Gas Sensing, Ultra-Sonication, Particle Size, Gas Sensitivity.

1. INTRODUCTION

In the intricate landscape of industrial processes and natural occurrences, the presence of hazardous gases is an ever-looming concern [1– 4]. The hazardous gases not only contaminate the environment but also severely affect the quality of life on the planet [5–7]. Thus, several gas sensors to detect numerous gases were fabricated based on the utilization of variety of functional nanomaterials and reported in the literature [8–11]. Hydrogen Sulfide (H_2S), a colorless and toxic gas, is a byproduct of natural gas, volcanic emissions, and various industrial practices, including food processing, paper manufacturing, rayon production, and petroleum refineries [12]. Recognizable by its pungent odor reminiscent of rotten eggs, H_2S poses multifaceted risks to both human health and the environment. Exposure to this compound can result in skin irritation, eye discomfort, respiratory issues, and more severe conditions like convulsions, coma, headaches, dizziness, and weakness. Beyond its immediate health hazards, H_2S contributes to environmental degradation and climate change, necessitating robust monitoring and detection systems in workplaces where hydrogen sulfide is prevalent [12]. The imperative to ensure the safety of individuals working in environments with potential H_2S exposure has led to an escalating demand for advanced gas detection systems. These systems play a pivotal role in swiftly detecting

[1]Department of Physics, J.D. Patil Sangludkar Mahavidyalaya, Daryapur Dist. Amravati, 444803, India
[2]Department of Physics, Vidya Bharti Mahavidyalaya, Camp Amravati, 444602, India
[3]Department of Physics, Jagat Arts, Commerce and I.H.P. Science College, Goregaon Dist. Gondia 441801, India
[4]Department of Physics, Gopikabai Sitaram Gawande College, Umarkhed Dist. Yavatmal, 445206, India
[5]Department of Physics, Shri R.L.T. College of Science, Civil Lines, Akola, 444001, India
[6]Department of Biochemistry, College of Science, King Saud University, 11451, Riyadh, Saudi Arabia
[7]Natural Science Department, Community College, King Saud University, P.O. Box 11433, Riyadh, 11433, Saudi Arabia
*Author to whom correspondence should be addressed.
Email: sushildeo86@gmail.com
Received: 16 February 2024
Accepted: 1 March 2024

and quantifying the concentration levels of H_2S, enabling timely responses to potential threats. In this context, the exploration of materials suitable for efficient gas sensing has become paramount, and several nanomaterials such as nickel oxide, manganese oxide, tin oxide, silver oxide, and so on were used for the electrode and reported in the literature [13–16]. Among these materials, Zinc Oxide (ZnO) has emerged as a promising candidate [17]. While pure ZnO has demonstrated commendable gas-sensing capabilities, ongoing research endeavors are dedicated to refining its efficiency [18]. One avenue of exploration involves reducing the particle size of ZnO, with the aim of enhancing its gas-sensing properties. The unique chemo-resistive properties of ZnO, coupled with its classification as an n-type semiconductor, make it particularly suited for gas sensor applications [2]. The working principle of ZnO sensors revolves around the retention of oxygen atoms on the sensor's surface when exposed to free atmospheric oxygen. This mechanism induces the formation of a depletion region between Zn–O, leading to fluctuations in the resistance of the sensor element based on the concentration of gases [1, 2]. The effectiveness of ZnO-based gas sensors is intricately linked to the method employed during their synthesis. Various synthesis methods have been explored, each imparting distinct morphological structures to the resulting ZnO [1, 2]. Hydrothermal processes, involving specific conditions such as temperature and duration, have produced structures ranging from flower-shaped nanoparticles to nanowires. Other methods, including spray pyrolysis, microwave treatment, and solvo-thermal processes, have yielded diverse nanostructures like hollow spheres, nanoplates, nano-sheets, and nanorods [1, 2].

The choice of an optimal synthesis method is pivotal in the development of pure nano-sized ZnO gas sensors [1]. Extensive literature reports showcase the successful utilization of nano-sized pure ZnO as a gas sensor element [1]. Building upon this foundation, the present work aims to elevate the field by developing pure ZnO as a gas sensor, emphasizing its functionality at low operating temperatures. Additionally, the study hones in on the influence of ultra-sonication treatment on the synthesized ZnO. This treatment is envisioned to prevent material agglomeration, thereby contributing to the optimization of the gas sensor's efficacy.

This research addresses the critical need for advanced gas sensors, particularly for H2S detection. By exploring the gas-sensing properties of nano-sized pure ZnO and investigating the influence of various synthesis methods and ultra-sonication treatment, the study endeavors to contribute significantly to the development of highly efficient, cost-effective gas sensors. The ultimate goal is to enhance workplace safety, mitigate environmental risks, and fortify our ability to respond to potential gas-related threats with speed and precision.

2. EXPERIMENTAL DETAILS

2.1. Synthesis of Powder and Paste Preparation

In the pursuit of precision and scientific rigor, the synthesis of Zinc Oxide (ZnO) nanostructures and the preparation of thixotropic adhesive paste were carried out with meticulous attention to detail. Analytical-grade chemicals were employed to ensure the accuracy and reliability of the experimental outcomes. The process commenced with the disintegration of Zinc nitrate hexahydrate [$Zn(NO_3)_2.6H_2O$] in distilled water, resulting in a 0.15 M solution. Gradually, a 0.5 M water-based solution of Sodium hydroxide [NaOH] was introduced dropwise into the aqueous solution, with continuous stirring. The ensuing white solution underwent a 12-hour storage period at 75 °C, followed by a natural cooling phase at room temperature for an additional 12 hours. Subsequently, the white solution was carefully collected in a beaker.

To enhance the characteristics of the synthesized ZnO nanostructures, sonication was employed using a Sonicator obtained from Oscar Ultrasonic Pvt. Ltd. Various durations of sonication—10 minutes, 20 minutes, and 30 minutes—were applied to distinct samples. After sonication, the final product was obtained through centrifugation, followed by thorough cleaning with alcohol and distilled water. The cleaned product was then dried for two hours at 80 °C in a vacuum oven [19, 20]. Additionally, to ensure the removal of any impurities, the synthesized powder underwent a heat treatment in a muffle furnace at 800 °C for 8 hours, resulting in a highly pure ZnO nanostructure with a proportionally higher yield. The synthesized ZnO nanostructures were categorized based on the duration of sonication: 0 min ZnO (S0), 10 min ZnO (S1), 20 min ZnO (S2), and 30 min ZnO (S3).

To facilitate the preparation of thixotropic adhesive paste, organic compounds, including 2-(2-Butoxyethoxy) ethyl acetate, 3-methoxybutyl acetate, and DEG monobutyl ether, were blended with the synthesized pure Zinc oxide. The mixture was further enriched with ethylated cellulose powder, carefully proportioned to achieve the desired consistency and properties for the subsequent preparation of thick films.

2.2. Thick Film Preparation for Measurements

The next phase involved the application of the prepared ZnO in the form of thick films on a glass substrate, employing the screen printing technique. Following this, the thick films underwent a critical exposure for 6 hours at 500 °C. This exposure, often referred to as the firing process, served the dual purpose of removing the organic binder and inducing crucial chemical reactions on the surface of the film [21]. The reactions during the firing process played a pivotal role in determining the physical and electrical properties of the thick films. For further characterization and electrical connectivity, silver paste was meticulously applied at both ends of the thick films, creating robust electrical contacts.

2.3. Specifications of the Gas Sensing Unit

A bespoke system was designed and assembled to comprehensively study the gas-detecting characteristics of the fabricated thick film in the presence of test gases [21]. This innovative system facilitated not only the evaluation of sensing responses but also the creation of a realistic environment akin to a working gas sensor. The system featured a gas chamber, a sample holder, a voltage source cum pico ammeter, a temperature controller, and a gas injection system employing a mass flow controller (MFC). This set-up allowed for the controlled variation of atmospheric composition, precise electrical measurements, and regulated sample heating.

2.4. Characterization Techniques

To gain a comprehensive understanding of the synthesized samples, various characterization techniques were employed, including X-ray Diffraction (XRD), Energy Dispersive Spectroscopy (EDS), and Transmission Electron Microscopy (TEM). These techniques played a pivotal role in elucidating the crystal structure, crystal size, purity, and morphological properties of the synthesized ZnO nanostructures.

2.5. Measurement of Thickness

The thickness of the prepared ZnO films was a crucial parameter influencing their structural and electrical properties. Employing the Marutek TF32 Measurement System, the thickness dimensions of all pure ZnO thick film samples were meticulously measured. The observed thicknesses fell within a narrow range of 31 to 35 μm, demonstrating a consistent and uniform thickness across all prepared films. This precise control over thickness provided a solid foundation for subsequent characterizations and analyses.

3. RESULTS AND DISCUSSION

3.1. Structural and Morphological Characterizations

XRD Analysis: X-ray diffraction (XRD) was employed to delve into the crystal structure, crystalline size, and purity of the synthesized Zinc Oxides. The XRD patterns, depicted in Figure 1, exhibited distinct peaks indicative of the hexagonal wurtzite structure of ZnO. The greater peak intensities observed in the XRD patterns suggested enhanced crystallinity in the synthesized ZnO samples. XRD patterns of ZnO nanostructures with different sonication time show parallel results. Using PDXL software which provided with Rigaku Minflex 600 model, confirms that material does not contains any impurity. In quantitative analysis of S_0, it found that phase name of material is zinc oxide. The Scherrer equation, mentioned below, was applied to estimate the crystalline size, revealing the approximate mean crystallite size for each sample [22],

$$D = \frac{K\,\lambda}{\beta \sin\theta}$$

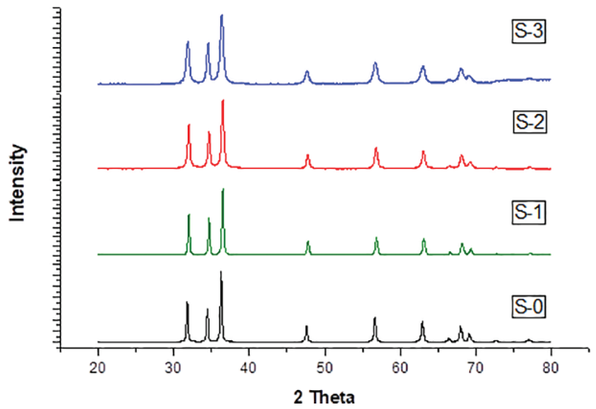

Fig. 1. Typical XRD pattern for the prepared S_0, S_1, S_2 and S_3 samples.

where λ is the wavelength of radiated beam (1.5406 A^0), β is the FWHM of the curve in radians, θ is the diffraction angle and Scherrer constant (k). The mean crystallite size was estimated from (101) peak. As illustrated in Table I, the crystallite size decreased with an increase in sonication time, indicating a correlation between sonication duration and particle size reduction.

TEM Analysis: Surface Topography: Transmission electron microscopy (TEM) was employed for a detailed investigation of the surface topography of the synthesized ZnO powders. As depicted in Figure 2(a), the TEM image illustrated the presence of nanospheres forming larger crystals. The ZnO powder exhibited a combination of nanoparticles and nanospheres, showcasing an average crystallite size of less than 50 nm. The TEM analysis provided valuable insights into the morphology of the synthesized ZnO, highlighting the efficiency of the sonication process in creating nanospheres and nanoparticles. The average crystallite size, as revealed by TEM, complemented the information obtained through XRD analysis, providing a comprehensive understanding of the structural features of the synthesized ZnO materials.

EDS Analysis: Energy dispersive spectroscopy (EDS) was conducted on the S3 sample for elemental analysis and observed results are shown in Figure 2(b). The EDS investigation revealed a lack of impurity elements in the ZnO-thick film. The non-stoichiometric nature of ZnO films was evident from the elemental analysis, showcasing an excess of zinc and a distorted band structure. This deviation from stoichiometry contributes to the formation of an n-type semiconductor, influencing the conductivity of the

Table I. Crystallite size for S_0, S_1, S_2 and S_3 samples.

Sr. No	Illustration	2θ (°)	FWHM Value (°)	Crystallite Size (nm)
1	S_0	36.25	0.1022	85.46
2	S_1	36.41	0.1235	70.76
3	S_2	36.45	0.1485	58.85
4	S_3	36.33	0.1795	48.67

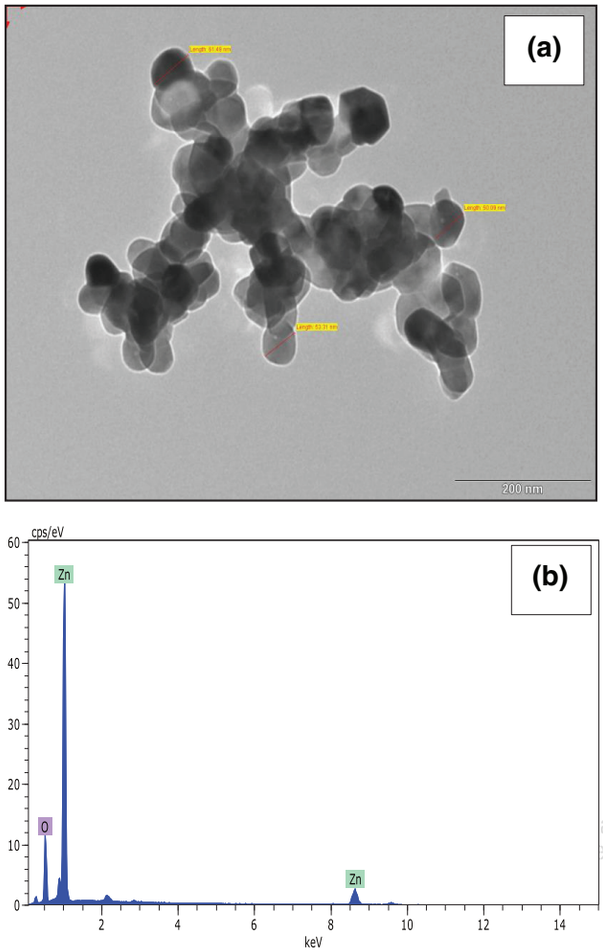

Fig. 2. (a) Typical TEM image and (b) EDS spectra of Prepared S_3 thick film.

material. The elemental composition of the ZnO-thick film (S3) is detailed in Table II.

The integration of XRD, EDS, and TEM analyses facilitated a multi-faceted characterization of the synthesized ZnO nanostructures. The results underscored the impact of sonication on crystallite size, affirmed the non-stoichiometric nature of ZnO films, and provided a detailed view of the morphology at the nanoscale. These findings contribute to advancing the understanding of ZnO materials for potential applications in gas sensing and related fields.

3.2. Impact of Ultra-Sonication on Particle Size

The investigation into the impact of ultra-sonication on particle size focused on understanding how varying sonication periods influenced the mean crystallite size [19–23]. As detailed in Table III, an intriguing correlation emerged, demonstrating a clear reduction in the mean crystallite size with an increase in sonication time.

The X-ray diffraction (XRD) patterns depicted in the study revealed that ultrasonic radiation treatment did not significantly alter the diffraction peaks. This observation suggests that the bombardment of ultrasonic radiation, while not inducing noticeable changes in the diffraction pattern, had a substantial impact on the crystallite size. The mechanical influence of radiated ultrasonic radiation created an immiscible state and induced stirring effects. These effects, detailed in Table III, highlighted the preventive role of ultra-sonication in the growth and aggregation of crystals [23]. The reduction in crystallite size can be attributed to the disruptive forces introduced by the ultrasonic radiation, preventing the crystalline structures from reaching larger sizes and promoting a more dispersed state. The results underscore the efficacy of ultra-sonication in controlling and reducing the crystallite size, offering valuable insights into the potential applications of this technique in tailoring the properties of ZnO materials for specific purposes, such as gas sensing.

3.3. H_2S Gas Sensing Properties

The assessment of H_2S gas sensing properties involves the critical examination of gas response or sensitivity (S), a pivotal metric represented by the ratio of the change in sensor current upon exposure to the target gas (I_g) to the initial current recorded in ambient air (I_a), as expressed by below Equation:

$$S = \frac{Ig}{Ia}$$

This parameter is fundamental in understanding the sensor's dynamic response to the introduction of H_2S, crucial for its effective operation. Furthermore, the concept of selectivity, which gauges the sensor's ability to discern and react to the target gas in the presence of other gases, is explored. The selectivity coefficient, denoting the maximum retaliation of the target gas concerning other gases under optimal conditions, provides insights into the sensor's specificity.

3.4. Thick Films of Pure ZnO: Sensing Performance

In the exploration of the sensing performance of the pure ZnO thick films, a comprehensive analysis was conducted on all fabricated samples under a standardized

Table II. Composition of ZnO thick film (S_3-Sample).

Element	Atomic number	Mass%	At. wt.%
Zn	30	74.84	69.44
O	8	25.16	23.55

Table III. Comparison of crystallite size with sonication time.

Sr. No	Sample	Crystallite size (nm)	Sonication time interval (min)
1	S0	85.46	0
2	S1	70.76	10
3	S2	58.85	20
4	S3	48.67	30

concentration of 100 ppm H_2S gas. This investigation encompassed a range of operational temperatures, scrutinizing the dynamic behavior of these ZnO-based sensors. Figure 3 graphically illustrates the nuanced relationship between gas response and working temperature for each thick ZnO film sensor element in the presence of H_2S gas. The depicted graph elucidates a compelling trend: as the operational temperature ascends, the gas sensitivity of the ZnO-based sensor elements towards H_2S gas undergoes a discernible augmentation. This escalation reaches a pinnacle, representing the optimal operating temperature, beyond which the sensitivity gradually diminishes. Notably, the S3 sample emerges as a standout performer, exhibiting the maximum gas response to H_2S among all other samples. The superiority of the S3 sample's performance can be attributed to its distinctive characteristics, notably its high surface-to-volume fraction facilitated by the smallest crystalline size among the samples. This is a pivotal observation as the heightened surface-to-volume fraction translates to an increased availability of active regions crucial for the gas sensing mechanism [24, 25]. The corroboration of these findings is evident in both XRD graphs and TEM images of the S3 sample, emphasizing the coherence between structural attributes and sensing efficiency. This insightful analysis underscores the intricate interplay between structural properties, operational conditions, and gas response. The optimal performance at a specific temperature threshold highlights the delicate balance required for efficient gas sensing applications. The prominence of the S3 sample not only accentuates its potential for enhanced sensing capabilities but also underscores the significance of tailored structural design in optimizing sensor performance. These findings contribute valuable insights to the burgeoning field of gas sensing technologies, steering advancements toward more efficient and tailored sensor designs.

3.5. Effect of Gas Level at Room Temperature: H_2S Gas

In-depth scrutiny of the S3 thick film sensor's gas response unfolds as Figure 4 delineates its behavior across varying concentrations of H_2S gas at room temperature (423 K). This analysis provides a comprehensive depiction of the gas response fluctuations within the ppm range (100–600 ppm), with particular emphasis on the S3 thick film's performance. The graph vividly portrays the characteristic gas response variations of the S3 thick film sensor concerning different H2S concentrations. Notably, a remarkable surge in response values is observed, peaking at 400 ppm. This distinctive pattern delineates the active range of the S3 thick film sensor, showcasing optimal sensitivity within the concentration bracket of 100 to 400 ppm. The underlying principle for this response behavior lies in the accumulation of an unimolecular layer of H_2S gas molecules on the sensor's surface. This concentration-dependent interaction generates a heightened gas response, indicating a robust sensitivity of the S3 thick film within its active range. However, as H_2S concentrations escalate beyond 400 ppm, a saturation point is discerned. At higher concentrations, a multi-layered assembly of gas molecules occurs, resulting in diminished responsiveness. Excess gas molecules, unable to reach the surface's active sites, remain unutilized, curtailing a substantial increase in the response. This observed response pattern aligns with established theories in gas sensing literature [26, 27], underlining the nuanced dynamics between gas concentrations and sensor reactivity. The delineation of the S3 thick film sensor's active range not only elucidates its optimal operating parameters but also provides critical insights for potential applications in environments with controlled H_2S concentrations. These findings contribute substantively to the comprehension of gas sensing mechanisms, offering practical considerations for optimizing sensor performance within defined concentration thresholds. The detailed analysis underscores the importance of understanding concentration-dependent

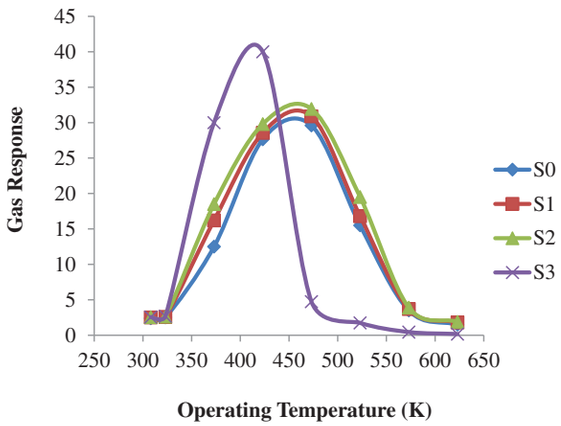

Fig. 3. H_2S gas response towards ZnO thick films.

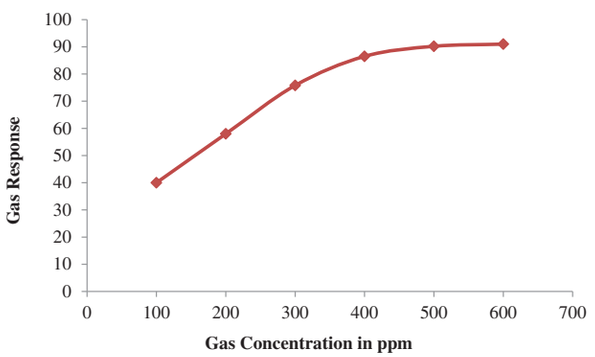

Fig. 4. Gas response of S_3 thick film sensor as a function of H_2S gas concentration at 423 K.

response dynamics, fostering advancements in gas sensing technology and tailored sensor applications.

3.6. Selectivity for H_2S Against Other Gases

Figure 5 illuminates the selectivity profile of the S3-thick film, shedding light on its discerning responsiveness to various gases under scrutiny, with a particular emphasis on its heightened sensitivity to H_2S gas. The results underscore the S3-thick film's noteworthy selectivity, showcasing a more pronounced response to H_2S in comparison to other investigated gases.

Gas sensing mechanisms primarily hinge on two fundamental approaches: surface adsorption of atmospheric oxygen and/or direct reactivity between lattice or interstitial oxygen and test gases. The adsorption of oxygen ions from the air diminishes the electrical current in semiconductor materials, as expressed in the equation:

$$O_2 + e^- \rightarrow 2O^-$$

Conversely, ambient reducing gases (R) interact with oxygen ions, capturing electrons and enhancing the semiconductor's current:

$$R + O^- \rightarrow RO + e^-$$

This interplay results in the dispersion of gaseous molecules into ions across the semiconductor surface, engaging with the oxygen ion lattice. The ionized reducing gas, provided the activation energy is sufficient, permeates the semiconductor's surface. This intricate mechanism involves interstitial oxygen ions and oxygen vacancies within the defect structure, articulated through Kroger-Vink notations [27]:

$$O_o \rightarrow V_O{}^{++} + O_I^{--}$$

$$R + O_i^{--} \rightarrow RO + 2e^-$$

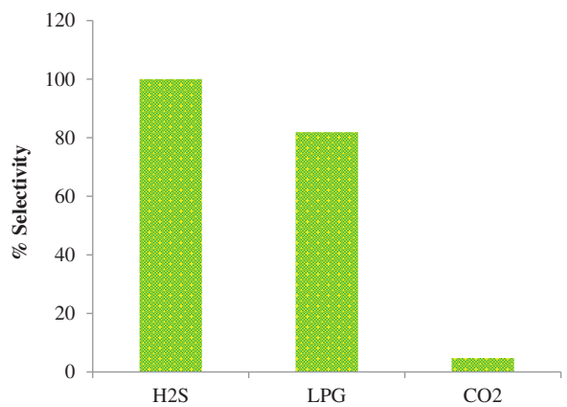

Fig. 5. Selectivity of different gases against H_2S gas at 423 K for S_3 thick films.

Here, O_o signifies oxygen at lattice position, V_O^{++} represents the lattice's oxygen vacancy, and O_i $O_1{}^{--}$ denotes oxygen in between.

The current amplifies as the reducing gas reacts with interstitial oxygen, yielding two electrons in the sensor material. The ZnO sensor operates by adsorbing oxygen onto an available surface site, and the reaction between the deposited oxygen and the test gas H_2S induces a change in the sensor material's current:

$$ZnO + H_2S \rightarrow ZnS + H_2O$$

ZnS exhibits superior electronic conductivity compared to ZnO. Pre-adsorbed oxygen ions from the sensor surface may induce a decrease in sensitivity factor (R) at higher temperatures [28, 29]. In comparative analysis, the S3 sample manifests a notably reduced response to LPG gas, underscoring the distinctive sensing mechanisms inherent in detecting different gases. These findings not only enhance our understanding of gas sensing intricacies but also contribute to the strategic development of sensors with tailored selectivity and heightened sensitivity, fostering advancements in diverse applications of gas sensing technologies.

4. CONCLUSION

In summary, the investigation into synthesized ZnO samples through a chemical route method followed by sonication has yielded significant insights. The findings establish the highly crystalline nature of the samples, characterized by a hexagonal wurtzite structure. The ZnO-thick films, meticulously prepared, exhibit a consistent thickness falling within the range of 31 to 35 μm. Utilizing the XRD technique, the mean crystallite size of the S3 sample is determined to be 48.67 nm. The analysis affirms the presence of Zn and O elements exclusively, attesting to the purity of the synthesized material without any discernible impurities. Intriguingly, XRD analysis unravels a compelling correlation: as sonication time increases, crystallite size decreases. The EDS analysis of the S3 thick film further corroborates the elemental composition, highlighting the exclusive presence of Zn and O. The TEM image of the S3 sample's powder unveils a distinctive composition, characterized by a plethora of nanospheres adeptly accumulating to form larger crystals. The average crystalline size measures less than 50 nm, underscoring the nanoscale attributes of the synthesized material. The sensor element derived from the S3 sample exhibits a commendable gas response across various tested gases, a characteristic attributed to its reduced crystalline size. Particularly noteworthy is its moderate gas response to H_2S, coupled with relatively moderate selectivity against CO_2 gases. The active zone of the S3 sensor for H_2S gas is discerned between 100 and 400 ppm, presenting a promising

operational range. The systematic exploration and characterization of ZnO samples, coupled with the development of sensor elements, lay the groundwork for enhanced understanding and application of gas sensing technologies. The findings not only underscore the importance of synthesis methodologies but also pave the way for tailored sensor designs with improved selectivity and sensitivity, promising advancements in diverse gas sensing applications.

Conflict of Interest

Authors declare no conflict of interest.

Acknowledgments: Authors are thankful to Materials Research Laboratory, Vidya Bharti Mahavidyalaya Amravati Maharashtra, Bharat, for availing research laboratory equipment. A researcher funding project number (RSP2024R406) from King Saud University in Riyadh, Saudi Arabia, has also provided funds for this work.

References and Notes

1. Kumar, R., Al-Dossary, O., Kumar, G. and Umar, A., **2015**. Zinc oxide nanostructures for NO_2 gas–sensor applications: A review. *Nano-Micro Letters*, *7*, pp.97–120.
2. Nadargi, D.Y., Umar, A., Nadargi, J.D., Lokare, S.A., Akbar, S., Mulla, I.S., Suryavanshi, S.S., Bhandari, N.L. and Chaskar, M.G., **2023**. Gas sensors and factors influencing sensing mechanism with a special focus on MOS sensors. *Journal of Materials Science*, *58*(2), pp.559–582.
3. Li, N., Yu, L. and Zhang, H., **2023**. 2D SnO2/g-C3N4 heterojunctional nanocomposite-based acetone sensor. *Journal of Nanoelectronics and Optoelectronics*, *18*(12), pp.1419–1426.
4. Kundara, S.K., Verma, M.K., Bidiyasar, R., Chawla, K., Lal, N., Lal, C., Tripathi, B., Jakhar, N., Mahmoud, M.H. and Akhtar, M.S., **2023**. Tailoring the structural, optical and electrical properties of Mn doped ZnO thin films for gas sensing response. *Science of Advanced Materials*, *15*(6), pp.772–780.
5. Guo, K., Zhou, X., Zhang, Z. and Qu, G., **2023**. A novel hierarchical nickle oxide gas sensor for monitoring the volatile organic compounds in car cabs. *Journal of Nanoelectronics and Optoelectronics*, *18*(6), pp.753–760.
6. Umar, A., Kumar, R., More, P.S., Ibrahim, A.A., Algadi, H., Alhamami, M.A., Baskoutas, S. and Akbar, S., **2023**. Polyethylene glycol embedded reduced graphene oxide supramolecular assemblies for enhanced room-temperature gas sensors. *Environmental Research*, *236*, p.116793.
7. Luo, Q., Ma, Z.W., Zou, J.F., Yang, H., Liu, Z.H. and Qiu, Y., **2022**. First-principles study on adsorption of CO_2 and SO_3 in flue Gas by Sc doped MoS_2 sensor. *Science of Advanced Materials*, *14*(5), pp.883–890.
8. Umar, A., Ibrahim, A.A., Algadi, H., Albargi, H., Alsairi, M.A., Wang, Y. and Akbar, S., **2022**. Supramolecularly assembled isonicotinamide/reduced graphene oxide nanocomposite for room-temperature NO_2 gas sensor. *Environmental Technology & Innovation*, *25*, p.102066.
9. Sun, H., Hua, Y. and Li, Z., **2023**. Preparation of three-dimensional NiO gas sensor for monitoring the indoor air of car cabs. *Journal of Nanoelectronics and Optoelectronics*, *18*(4), pp.479–485.
10. Shah, S., Hussain, S., Shaheen, A., Liu, G., Hashem, M., Alsarani, M.M., Akhtar, M.S., Tianyan, Y., Qiao, G. and Fouad, H., **2023**. Nanoparticles embedded In_2O_3 microspheres for selective and quantitative detection of NO_2 gas. *Science of Advanced Materials*, *15*(5), pp.625–633.
11. Bae, J.W., **2022**. Fabrication of sensor-on-wafer (SoW) temperature monitoring sensor. *Science of Advanced Materials*, *14*(4), pp.655–660.
12. Srivastava, J.K., Gupta, A. and Bhaskar, A.A., **2014**. Sensing behavior of CuO-doped SnO_2 thick film sensor for H_2S detection. *Int. J. Scientific and Technology Research*, *3*(5), pp.266–272.
13. Umar, A., Ibrahim, A.A., Algadi, H., Albargi, H., Alsairi, M.A., Wang, Y. and Akbar, S., **2021**. Enhanced NO_2 gas sensor device based on supramolecularly assembled polyaniline/silver oxide/graphene oxide composites. *Ceramics International*, *47*(18), pp.25696–25707.
14. Umar, A., Ibrahim, A.A., Kumar, R., Albargi, H., Zeng, W., Alhmami, M.A.M., Alsaiari, M.A. and Baskoutas, S., **2021**. Gas sensor device for high-performance ethanol sensing using α-MnO_2 nanoparticles. *Materials Letters*, *286*, p.129232.
15. Umar, A., Ibrahim, A.A., Kumar, R., Algadi, H., Albargi, H., Ahmad, F., Zeng, W. and Akhtar, M.S., **2021**. α-mno$_2$ nanowires as potential scaffolds for a high-performance formaldehyde Gas sensor device. *Coatings*, *11*(7), p.860.
16. Umar, A., Ammar, H.Y., Kumar, R., Almas, T., Ibrahim, A.A., AlAssiri, M.S., Abaker, M. and Baskoutas, S., **2020**. Efficient H_2 gas sensor based on 2D SnO_2 disks: Experimental and theoretical studies. *International Journal of Hydrogen Energy*, *45*(50), pp.26388–26401.
17. Umar, A., Singh, J., Ibrahim, A.A., Kumar, R., Rai, P., Rai, A.K., Algadi, H., Alhamami, M.A. and Elsddig, M.M., **2021**. Cauliflower-shaped ZnO nanostructure for enhanced NO_2 gas sensor application. *Science of Advanced Materials*, *13*(12), pp.2358–2363.
18. Zhou, Q., Zeng, W., Chen, W., Xu, L., Kumar, R. and Umar, A., **2019**. High sensitive and low-concentration sulfur dioxide (SO_2) gas sensor application of heterostructure NiO-ZnO nanodisks. *Sensors and Actuators B: Chemical*, *298*, p.126870.
19. Patil, A.V., Dighaykar, C.G., Sonawane, S.K., Shinde, U.P., Patil, S.J. and Borse, R.Y., **2010**. Study of microstructural parameters of screen printed ZnO thick film sensors. *Sensors & Transducers*, *117*(6), p.62.
20. Asokan, T., Nagabhushana, G.R. and Iyengar, G.N.K., **1988**. Improvement of non-linear characteristics of multicomponent ZnO-based ceramics containing Nb/sub 2/O/sub 5. *IEEE Transactions on Electrical Insulation*, *23*(2), pp.279–286.
21. Patil, D.R., Patil, L.A. and Patil, P.P., **2007**. Cr_2O_3-activated ZnO thick film resistors for ammonia gas sensing operable at room temperature. *Sensors and Actuators B: Chemical*, *126*(2), pp.368–374.
22. Patterson, A.L., **1939**. The scherrer formula for X-ray particle size determination. *Physical Review*, *56*(10), p.978.
23. Rataboul, F., Nayral, C., Casanove, M.J., Maisonnat, A. and Chaudret, B., **2002**. Synthesis and characterization of monodisperse zinc and zinc oxide nanoparticles from the organometallic precursor $[Zn(C_6H_{11})_2]$. *Journal of Organometallic Chemistry*, *643*, pp.307–312.
24. Frühberger, B., Grunze, M. and Dwyer, D.J., **1996**. Surface chemistry of H_2S-sensitive tungsten oxide films. *Sensors and Actuators B: Chemical*, *31*(3), pp.167–174.
25. Verma, V., Pandey, N.K., Singh, A., Singh, P., Gupta, P. and Yadav, B.C., **2022**. Liquefied petroleum gas (LPG) sensing of biphasic Cu_6Sn_5: SnO_2 nanocomposite thin-films. *Materials Chemistry and Physics*, *289*, p.126459.

26. Mitra, P., Chatterjee, A.P. and Maiti, H.S., **1998**. Zno thin film sensor. *Materials Letters*, *35*(1–2), pp.33–38.
27. Li, Z., Yu, J., Dong, D., Yao, G., Wei, G., He, A., Wu, H., Zhu, H., Huang, Z. and Tang, Z., **2023**. E-nose based on a high-integrated and low-power metal oxide gas sensor array. *Sensors and Actuators B: Chemical*, *380*, p.133289.
28. Marsal, A., Dezanneau, G., Cornet, A. and Morante, J.R., **2003**. A new CO_2 gas sensing material. *Sensors and Actuators B: Chemical*, *95*(1–3), pp.266–270.
29. Zhu, L., Rong, Q., Yang, Z., Zhang, W., Jiao, M., Song, J., Wang, C. and Guo, Y., **2022**. ZnO nanoparticle-based MEMS sensors for H_2S detection. *ACS Applied Nano Materials*, *5*(8), pp.11595–11604.